 doi:10.20944/preprints201612.0094.v1

Article

Synthesis, characterization and catalytic performance of well-ordered crystalline heteroatom mesoporous MCM-41

Jing Qin[1,2] and Baoshan Li[1]*

1. State Key Laboratory of Chemical Resource Engineering, Beijing University of Chemical Technology, Beijing 100029, China
2. Department of environmental protection and biological pharmacy, Beijing Industrial Technician College, Beijing 100023, China
*Corresponding author. Tel/Fax: +86 010 64445611.
E-mail address: bsli@mail.buct.edu.cn; qinjing1234@sohu.com

Abstract: The mesoporous heteroatom molecular sieve MCM-41 bulk crystals with the crystalline phase were synthesized via a one-step hydrothermal method using an ionic complex as template. The ionic complex template was formed by interaction between cetyltrimethylammonium ions and metal complex ion $[M(EDTA)]^{2-}$ (M=Co or Ni). The materials were characterized by X-ray diffraction, scanning electron microscopy, high-resolution transmission electron microscopy, N_2 adsorption–desorption isotherms, and X-ray absorption fine structure spectroscopy. The results showed that the materials possess a highly ordered mesoporous structure with the crystalline phase and possess high uniform ordered arrangement channels. The structure is in the vertical cross directions with a crystalline size of about 12 μm and high specific surface areas. The metal atoms were incorporated into the zeolite frameworks in the form of octahedral coordinate and have a uniform distribution in the materials. The amount of metal complexes formed by metal ion and EDTA is an essential factor for the formation of the vertical cross structure. Comparing to Si-MCM-41, the samples exhibited better conversion, higher selectivity for cumene cracking.

Key words: Bulk crystal mesoporous MCM-41; Heteroatom molecular sieves; Direct hydrothermal method

1 Introduction

By virtue of their high thermal and hydrothermal stability, microporous zeolites are widely used in industries as heterogeneous catalysts, particularly as solid acid catalysts in the fields of oil refining and petrochemistry [1]. Although the micropores of zeolites have often been described as having excellent potential for chemical functions, their pore size often limit the reaction rate and thus have an

 doi:10.20944/preprints201612.0094.v1

adverse effect on practical chemical processes [2-4]. In 1992, in an attempt to overcome this problem, Mobil Oil Corporation synthesized a family of mesoporous solids named as M41s [5], which possess an ordered arrangement of larger pores with diameters of 2–10 nm. However, the use of these materials as catalysts is hampered by their relative low thermal stability and weak acid strength [6, 7]. Therefore it would be of great interest to synthesize a new type of material combining the advantages of both mesoporous molecular sieves and zeolites [8, 9]. Up to the present, only a few studies have been published, for example, Karlsson et al. prepared MFI/MCM-41 composites using two templates [$C_6H_{13}(CH_3)_3NBr$ and $C_{14}H_{29}(CH_3)_3NBr$] and optimized the template concentrations and reaction temperature [10]. In the previous studies, we have reported synthesis and characterization of composite molecular sieves M_1-MFI/M_2-MCM-41 (M_1, M_2 = Ni, Co) and their catalytic properties for the hydrocracking of residual oil [11], and the preparation of micro–mesoporous FeCo-MFI/MCM-41 composites which gave a clear improvement in the hydrocracking of residual oil [12]. However the resulting materials are composites of zeolite crystallites embedded in a disordered mesoporous matrix. Kaliaguine et al. described a general method for the production of a new type of material with semi-crystalline zeolite mesopore walls [13]. Other attempts to crystallize the mesopore walls of mesostructure materials have resulted in the formation of materials with increased thermal stability and catalytic activity. For example, ITQ zeolites having a partially crystalline bimodal pore system with a combination of micropores and mesopores have been synthesized by delaminating the layered zeolite precursors MCM-22 and ferrierite [14]. However, none of these techniques yields a regular distribution of mesopores, let alone an ideal channel system of mesopores structurally connected with the regular micropores of the zeolite. Jiang et al. reported the synthesis of zeolite ITQ-43, which features a structurally hierarchical system of connected mesopores and micropores. Although high-resolution transmission electron microscopy (HR-TEM) did not show the mesopore features, evidence for the presence of mesopores was provided by automated electron diffraction tomography [15]. W. Chaikittisilp recently demonstrated a new approach for the construction of hierarchically organized zeolites by sequential intergrowth, for the first time, a complex and unusual morphology was observed for MFI zeolites [16].

In this paper, the bulk crystal heteroatom molecular sieves M-MCM-41 with the crystalline phase have been synthesized using a direct hydrothermal method. The materials possess the crystalline phase and high uniform ordered arrangement channels and high specific surface areas. This is a new type of crystalline mesoporous molecular sieves. In a typical synthesis condition, the three-dimensional crystal mesoporous MCM-41 was obtained.

2 Experiments

2.1.Materials.

Nickel nitrate hexahydrate [$Ni(NO_3)_2{\cdot}6H_2O$] (AR, Beijing Yili Fine Chemical

Preprints (www.preprints.org) | NOT PEER-REVIEWED | Posted: 18 December 2016 doi:10.20944/preprints201612.0094.v1

Product Limited Company, China) is used as Ni source. Cobalt nitrate hexahydrate [Co $(NO_3)_2 \cdot 6H_2O$] (AR, Shantou Xilong Chemical Limited Company, China) is used as Co source. Cetyltrimethyl ammonium bromide (CTAB, AR, Tianjin Jinke Fine Chemical Institute, China) is used as structure template. Ethylenediaminetetraacetate (EDTA, AR, Beijing Chemical Factory, China) is used as structure-directing agent. White carbon black (SiO_2, AR, Beijing Chemical Factory, China) is used as Si source and sodium hydroxide (NaOH, AR, Beijing Chemical Factory, China) is used to adjust the pH.

2.2.Synthesis.

The new crystalline sample of Cry-M (M=Ni, Co) is prepared through a direct hydrothermal synthesis method, and the detailed process is as following: A transparent solution of the ionic complex $[M (EDTA)]^{2-}$was made by dissolving disodium ethylenediaminetetraacetate solution and a certain amount of $M(NO_3)_2 \cdot 6H_2O$ in H_2O (10g) and mixing well. 4.5 g (12.3 mmol) of CTAB was dissolved in 34 g of H_2O at 70 °C. In another flask, 0.5 g (12.5 mmol) of sodium hydroxide dissolved in 15 g of H_2O was mixed with 2.25 g (37.5 mmol) of SiO_2 stirred for 0.5 h and then heated to 60 °C. The ionic complex $[M (EDTA)]^{2-}$and CTAB solutions were then added to the silica solution and the resulting mixture stirred for 0.5 h to form a homogeneous emulsion. After adjusting the pH to 11 using sodium hydroxide solution, the mixture was stirred for another 12 h. The mixture was then transferred into a Teflon-lined autoclave and heated at 160 °C under autogenous pressure for 96 h. The resulting solid was filtered, and washed with water until pH of the filtrate reached 7.0. After drying the sample overnight at 100 °C, the template was removed by calcination in air at 550°C for 5 h.

2.3.Characterization.

X-ray powder diffraction (XRD) patterns were recorded on a Philips X'Pert diffractometer equipped with a rotating anode, using Cu Kα radiation (λ = 0.1541 nm). The pore morphology of the samples was examined by high-resolution transmission electron microscopy (HRTEM) on a JEM-2100 microscope with an accelerating voltage of 200 kV. The crystal morphology was studied using a Hitachi S-4700 scanning electron microscope (SEM). The chemical compositions of the samples were measured by Optima 8000 Inductively Coupled Plasma (ICP). Nitrogen adsorption–desorption isotherms were obtained using a Quantachrome Autosorb-1 volumetric adsorption analyzer. The volume of the adsorbed N_2 was normalized to standard temperature and pressure. Prior to the measurements, the samples were degassed at 300 °C for 16 h. The X-ray photoelectron spectroscopy (XPS) analyses were conducted on an ESCALAB 250 spectrometer equipped with an Al Kα X-ray source. The carbon 1s peak at 284.6 eV was used as the reference for binding energies. X-ray absorption fine structure (XAFS) spectroscopy of the M (Ni, Co) K-edge of the samples was performed on the U7C beamline at the National Synchrotron Radiation Laboratory (NSRL) of China. The typical energy of the storage ring was 0.8 GeV with a maximum current of 250 mA. A Si (111) double

Preprints (www.preprints.org) | NOT PEER-REVIEWED | Posted: 18 December 2016 doi:10.20944/preprints201612.0094.v1

crystal monochromator was used. The data analysis of all the XAFS spectra was carried out using the IFEFFIT software.

3.Results and discussions

The samples were labeled as Cry-Ni and Cry-Co and the metal heteroatom contents of the samples measured by ICP are listed in Table 1.

Table 1 Textural properties of the samples

Sample	M contents wt.% (by ICP)	S_{BET} (m^2 g^{-1})	*Pore volume* (cm^3 g^{-1})	*Pore diameter* (*nm*)
Cry-Ni	7.88	273	1.12	5.43
Cry-Co	6.77	425	0.97	3.51

Low angle XRD patterns of the samples are presented in Figure 1. All samples show an intense broad diffraction peak at very low 2θ angle of 1.2 – 1.8°, with an overlapping broader feature at 2 – 7°, which can be respectively attributed to the (1 0 0) diffraction peak and the overlapping pair of (1 1 0) and (2 0 0) diffraction peaks, indicating that the samples have good structural order and obvious mesoporous structure of MCM-41 [17].

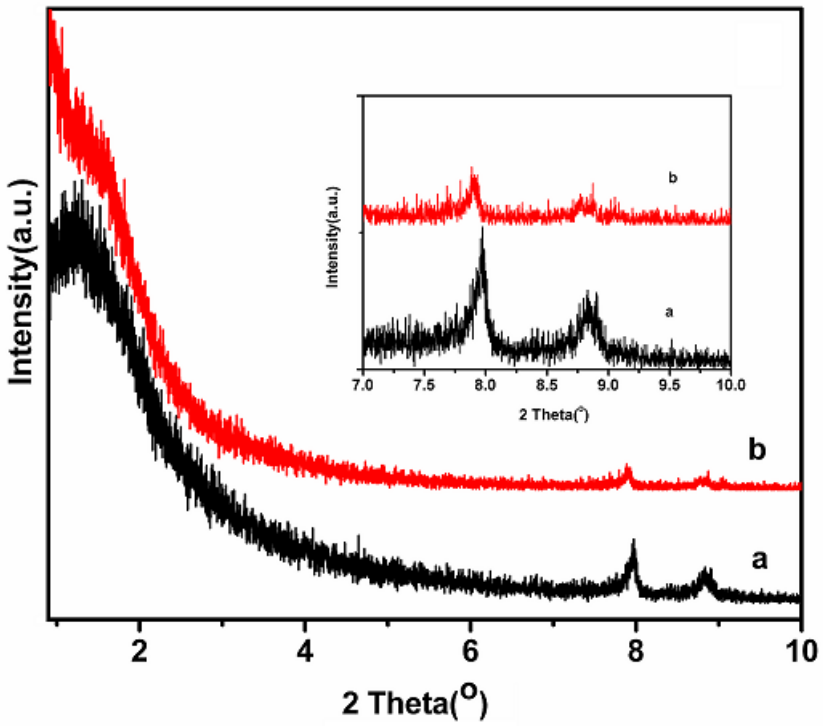

Figure 1 XRD patterns of the samples: (a) Cry-Ni, (b) Cry-Co.

The particle size and shape of the samples were investigated using SEM and the images are shown in Figure 2 (a and b). The results show that the samples have well-defined morphologies with a crystal structure, which are corresponding to the XRD results, and the crystalline sizes are about 12 μm with a uniform distribution. In addition, the materials possess a structure which is in the vertical cross directions. This is determined presumably by the structure of the metal complex.

 doi:10.20944/preprints201612.0094.v1

The SEM-mappings of the samples are also shown in Figure 2 (a* and b*), which can display the composition and distribution of elements in the samples. It is clear that all the samples (Cry-Ni and Cry-Co) have uniform distribution of elements and the metal
atoms (Ni and Co) were highly dispersed in the materials. After grinding with a ball mill, the samples were tested by HRTEM and the results were shown in Figure 2 (c and d). The images indicate that the materials exhibit a uniform pore size with a highly ordered pore structure and the characteristic of the long-range ordered symmetry of a mesophase. The ordered mesopores of the crystals can be easily observed in the HRTEM images.

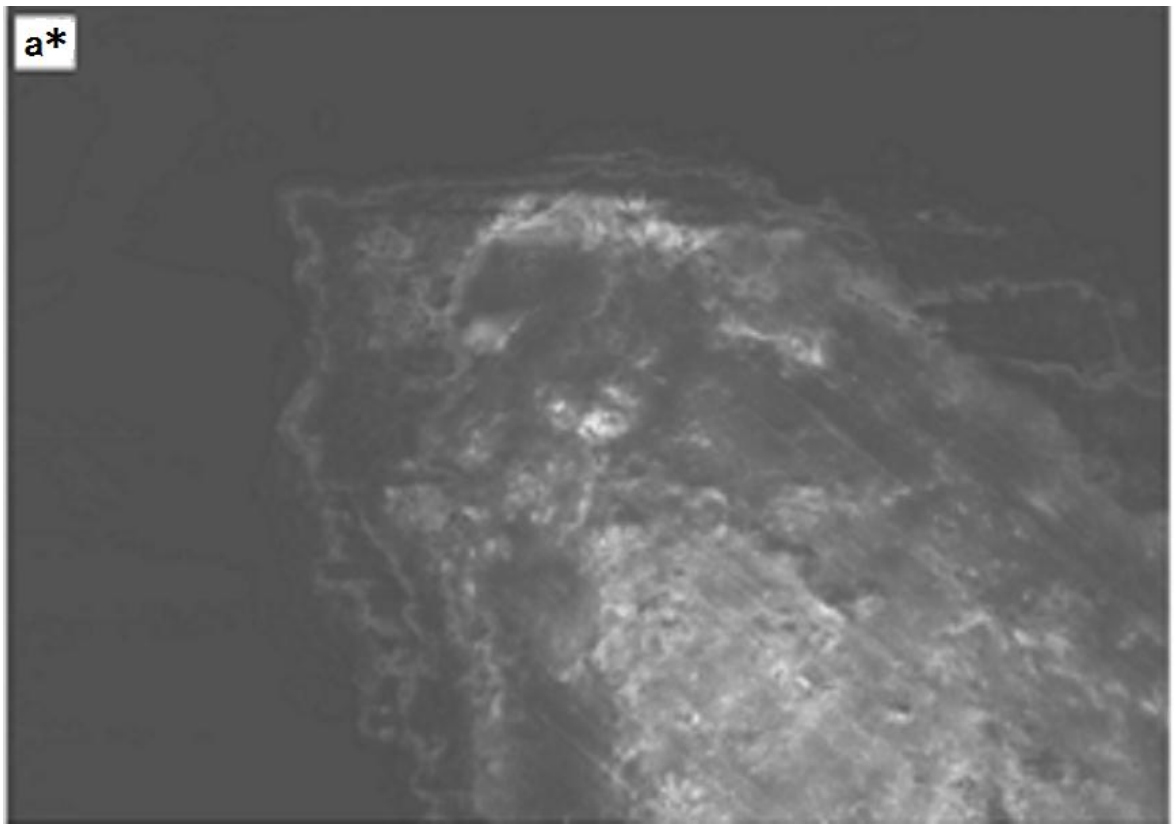

Preprints (www.preprints.org) | NOT PEER-REVIEWED | Posted: 18 December 2016 doi:10.20944/preprints201612.0094.v1

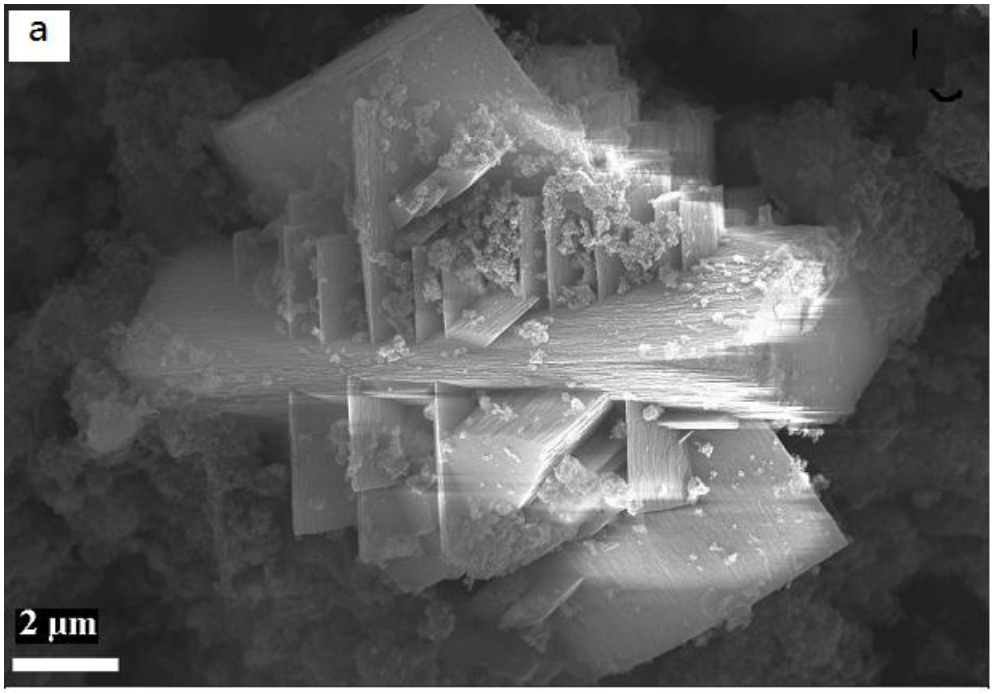

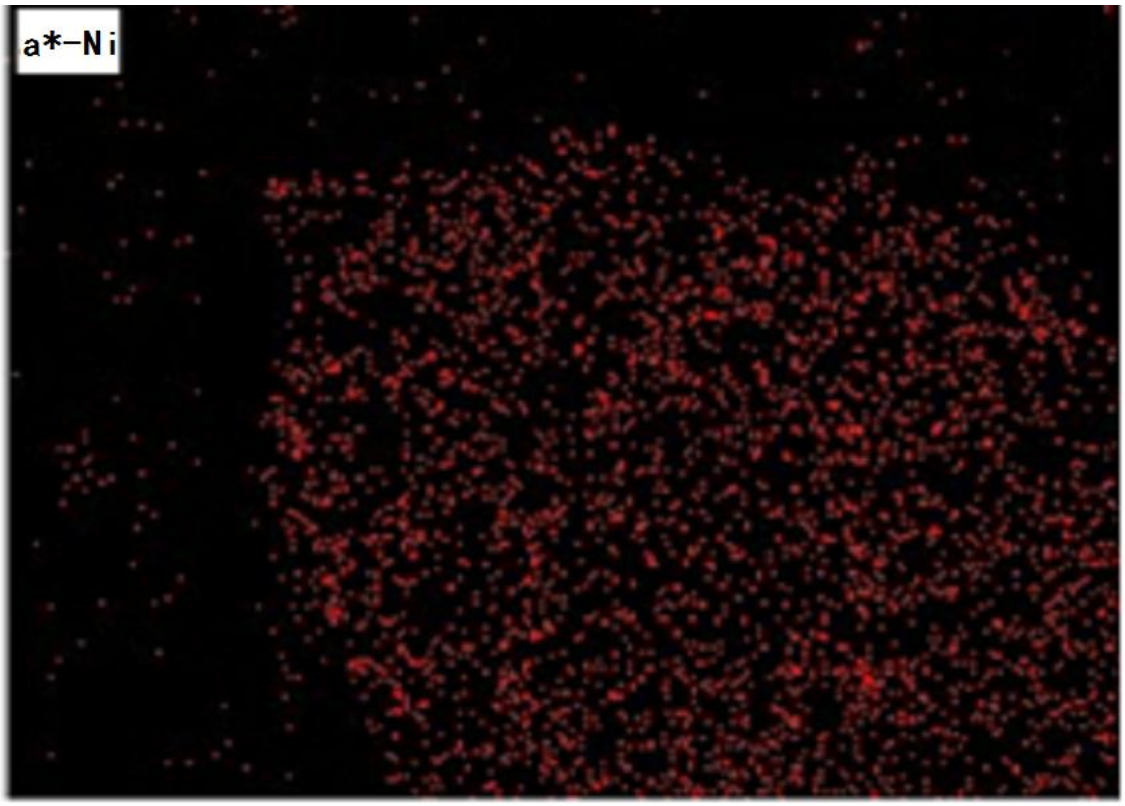

Preprints (www.preprints.org) | NOT PEER-REVIEWED | Posted: 18 December 2016 doi:10.20944/preprints201612.0094.v1

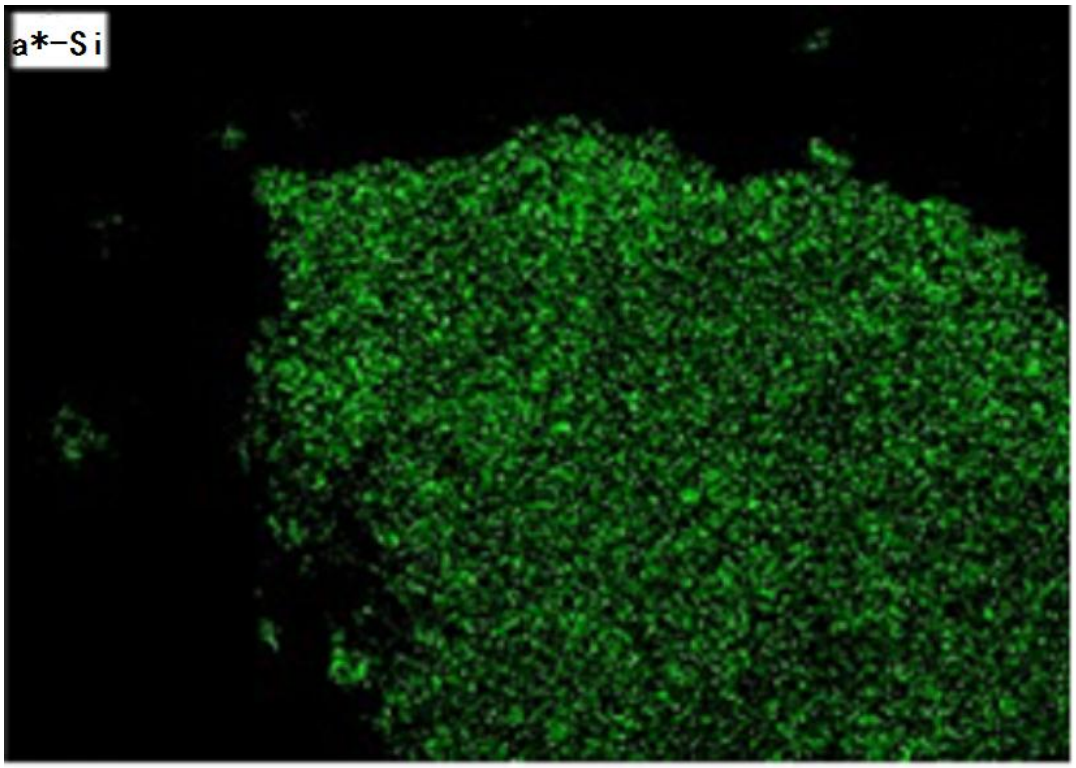

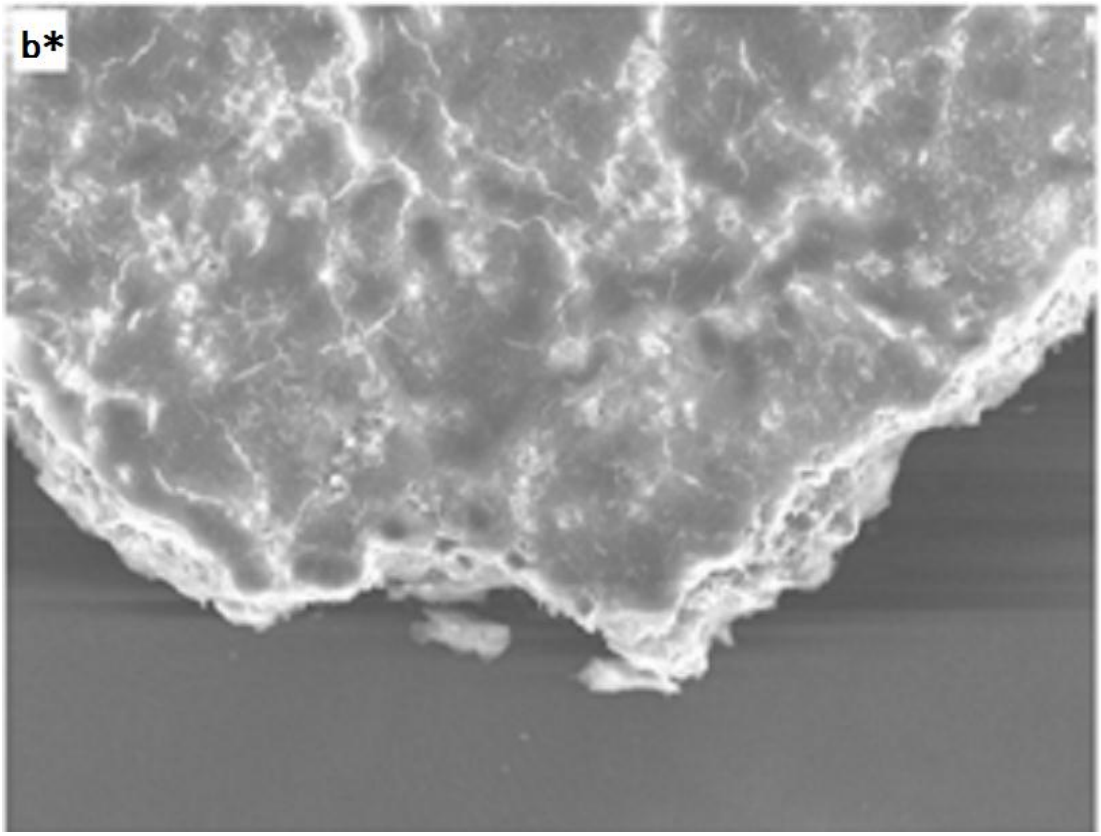

Preprints (www.preprints.org) | NOT PEER-REVIEWED | Posted: 18 December 2016 doi:10.20944/preprints201612.0094.v1

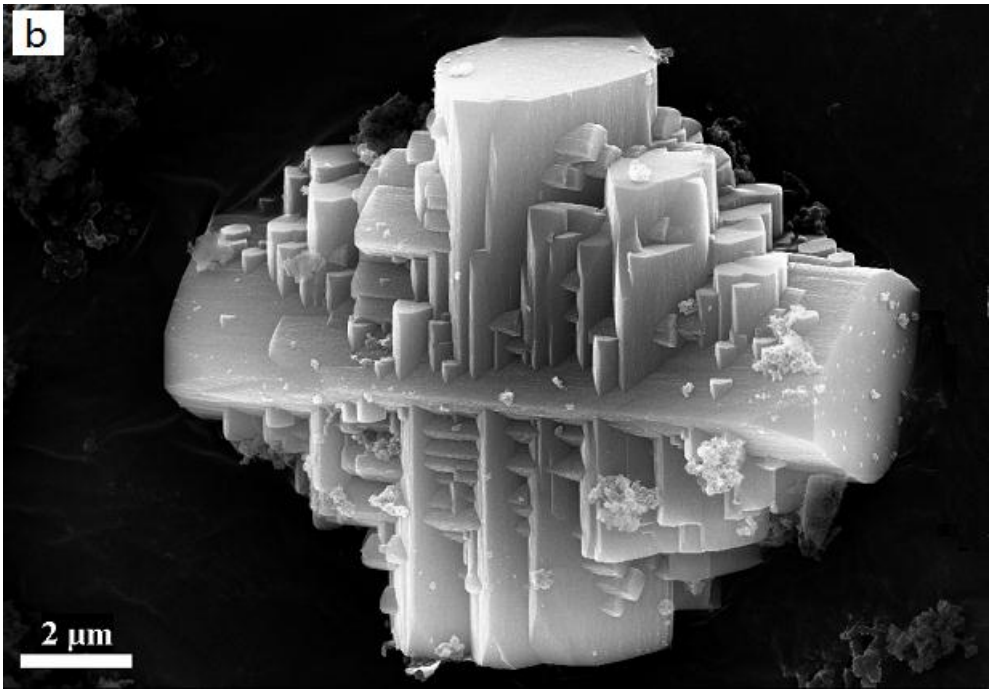

Preprints (www.preprints.org) | NOT PEER-REVIEWED | Posted: 18 December 2016 doi:10.20944/preprints201612.0094.v1

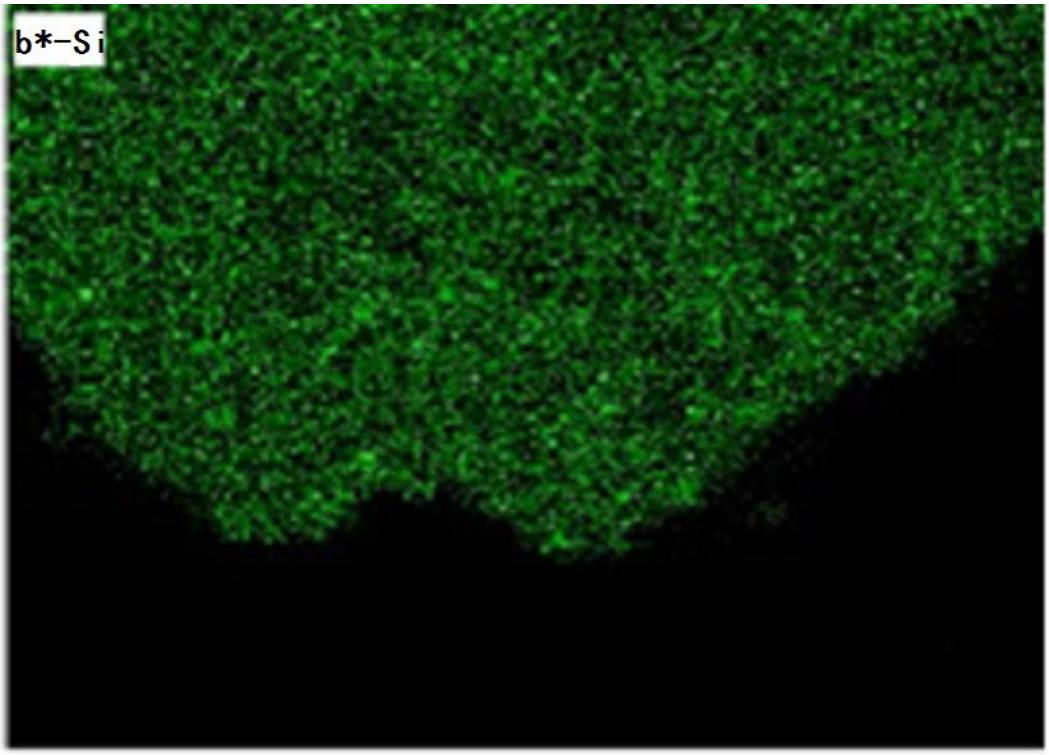

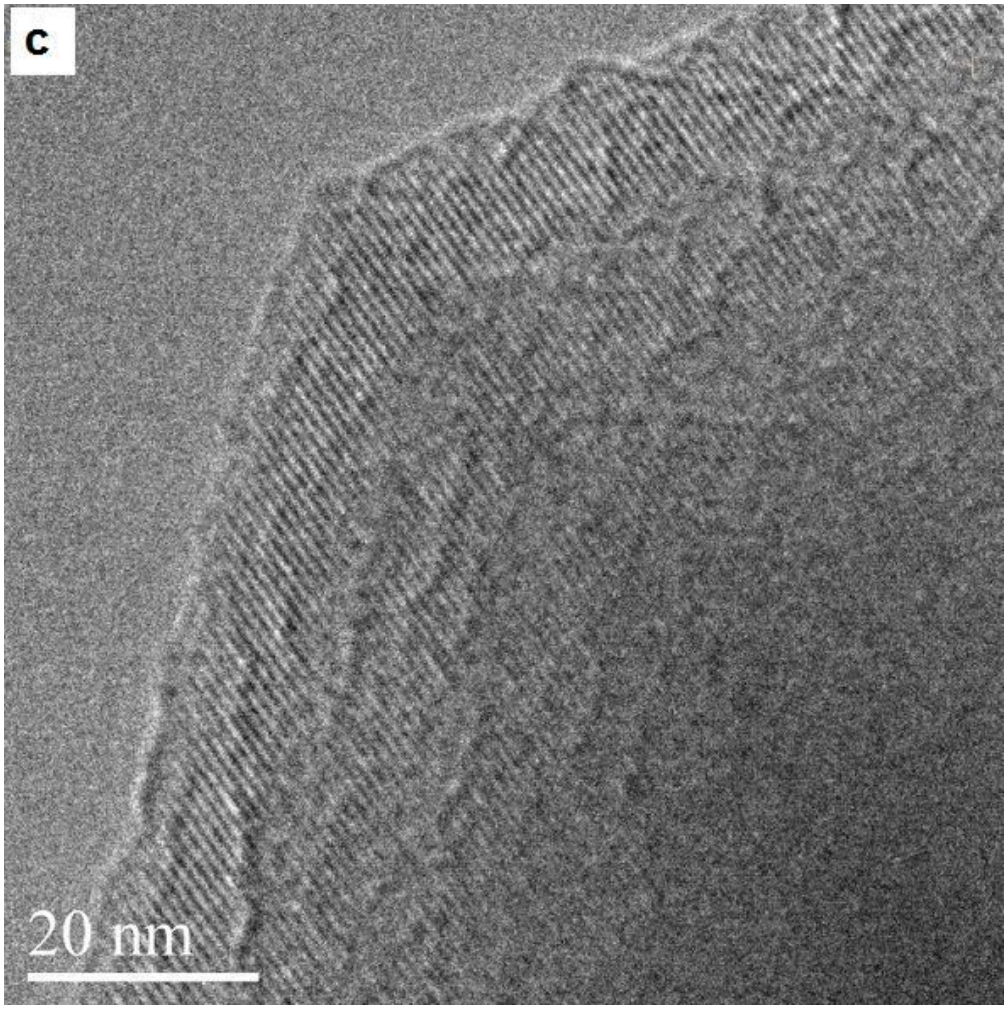

Preprints (www.preprints.org) | NOT PEER-REVIEWED | Posted: 18 December 2016 doi:10.20944/preprints201612.0094.v1

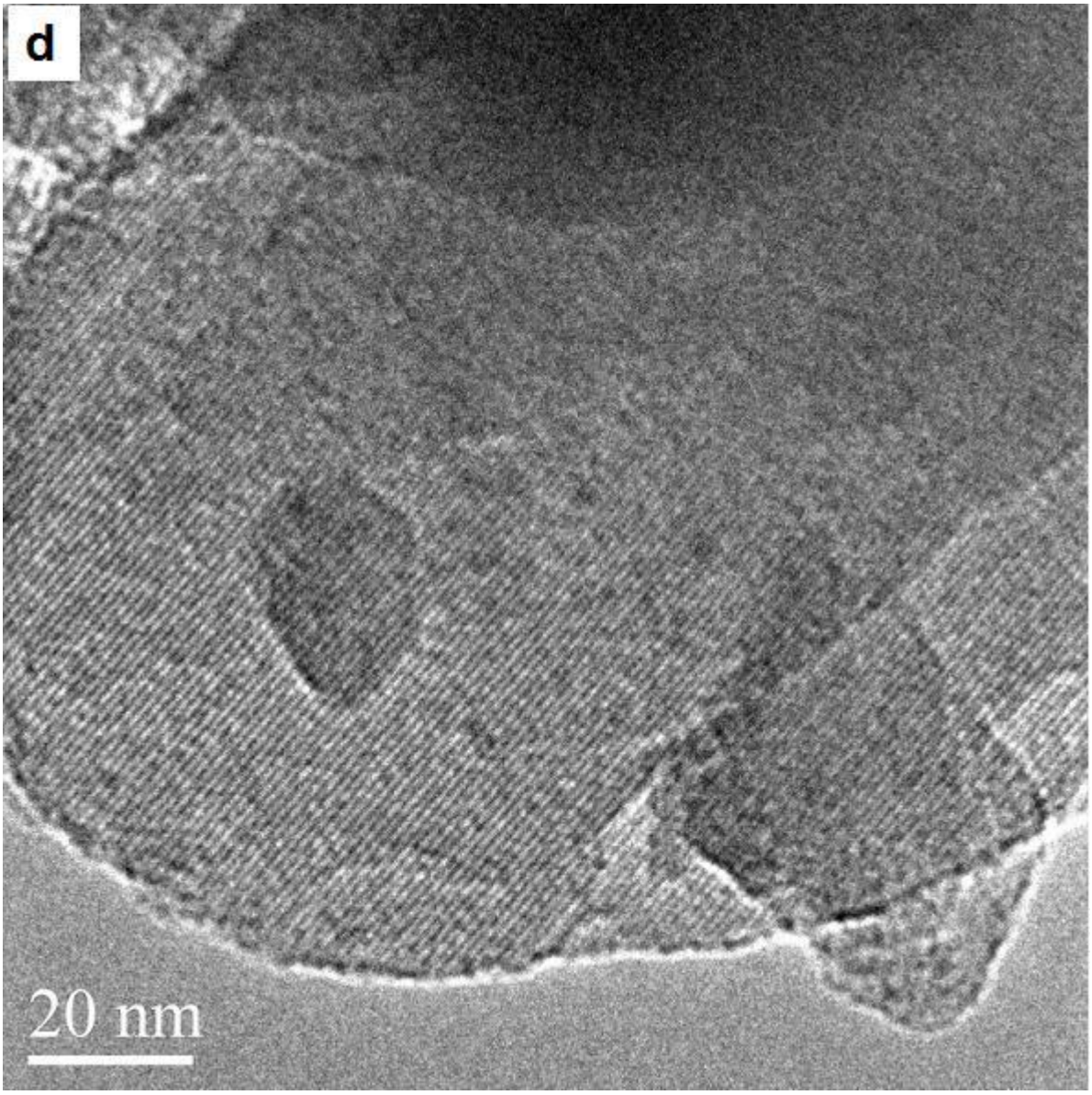

Figure 2 SEM images, SEM-mappings and HRTEM images of the samples Cry-Ni (a, a*, c) and Cry-Co (b, b*, d).

The handbook of X-Ray photoelectron spectroscopy showed the binding energy of NiO and CoO. The binding energy peak of NiO was between 854 eV and 855 eV. The peak of CoO and Co_3O_4 centered at 780 eV. Figure 3 is the XPS spectra of samples Cry-Ni and Cry-Co, and the insets are the de-convoluted Ni 2p3/2 and Co 2p3/2 spectra. As shown in Figure 3a, there is a predominant peak centered at 855.95 eV [18], indicating the strong interaction between nickel atom and the silica base, suggesting the nickel atoms incorporating into the silica framework[19], which corroborates the previous results; a peak centered at 781.55 eV existing in the Figure 3b, which is the characteristic peak of Co 2p2/3 [20], indicating cobalt atoms also incorporating into the silica framework.

Preprints (www.preprints.org) | NOT PEER-REVIEWED | Posted: 18 December 2016 doi:10.20944/preprints201612.0094.v1

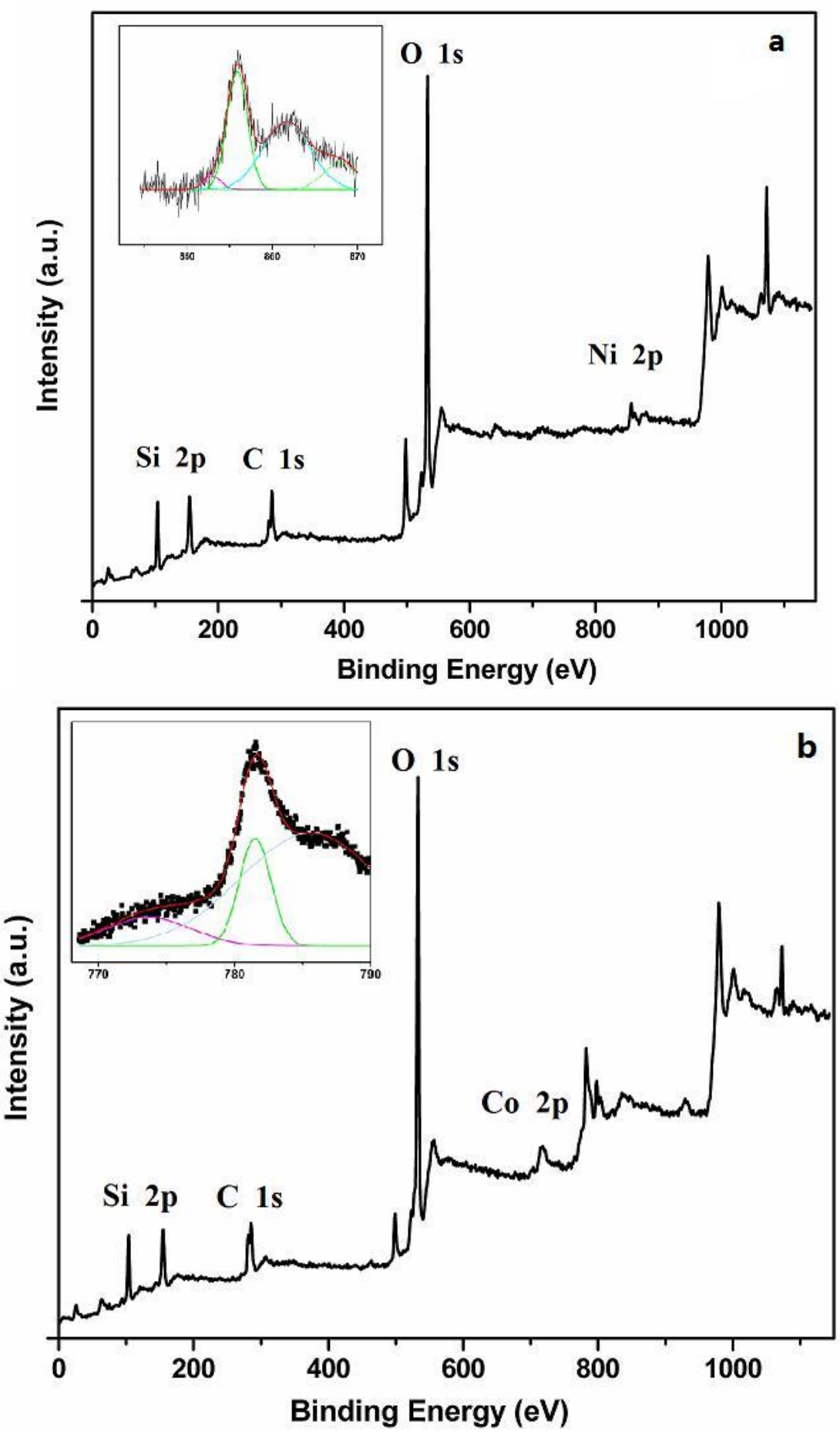

Figure 3 XPS spectra of the samples: (a) Cry-Ni, (b) Cry-Co.

 doi:10.20944/preprints201612.0094.v1

Figure 4 illustrates the XANES spectra of Cry-Ms. The corresponding spectra for metal oxides are given for comparison. The XANES pre-edge peak is attributed to the 1s-3d dipolar forbidden transition [21]. Principally, this 1s-3d forbidden transition gains additional intensity when the metal center is in non-centrally symmetric environment of through mixing of 3d and 4p orbitals caused by the breakdown of inversion symmetry due to the structure distortion. Figure 4a illustrates the X-ray absorption near-edge structure (XANES) spectra of NiO and Cry-Ni. The nickel atoms in Cry-Ni have similar pre-edge features to that of NiO, which indicates nickel exists as mainly Ni^{2+} in the material. Figure 4b displays the XANES spectra of CoO, Co_3O_4 and Cry-Co. The cobalt atoms in Cry-Co have the similar features with CoO, the result suggests Co^{2+} is existence in the sample. Note that the peaks are slightly shifted to a longer distance than standard samples because of the scattering phase shifts.

Extended X-ray absorption fine structure (EXAFS) spectroscopy [22] is one of the most powerful structural characterization methods, especial for interface-confined effects, due to its sensitivity to the three-dimensional short-range order (typically 0 – 8 Å) and chemical state, including near-neighbor species, distance (R), coordination number (N), and disorder in bond distance (σ^2). Figure 4a* shows the K^3-weighted spectra of Cry-Ni and NiO, which are the Fourier transformed of Ni K-edge EXAFS spectra in the range of k=2 – 6 Å. The peaks correspond to the distance between a Ni atom and its neighboring atoms. In the curve of NiO (a standard reference material), there are five peaks (① - ⑤) that can be ascribed to Ni-O ①, Ni-Ni ②, Ni-O ③, Ni-Ni Ni-Ni-O, Ni-O-Ni-O, Ni-O ④, and Ni-Ni ⑤ scattering paths, respectively. It is clear that the curve of Cry-Ni is different from the curve of NiO, although the two peaks ① and ② of Cry-Ni are similar with the peaks ① and ② of NiO, a new peak between the peaks ① and ② of Cry-Ni presents which is originated in the silicon atoms. The shape and intensity of the peaks ③, ④ and ⑤ are also different from that of NiO. The results show that the structure forms of Ni atoms in Cry-Ni are different from in NiO. The similar results were obtained in the sample Cry-Co. Figure 4b* presents the Fourier transforms of k^3-weighted of Co K-edge EXAFS spectra of Cry-Co, CoO and Co_3O_4 (standard reference materials). The curve of Cry-Co also presents two peaks ① and ②, which are similar with the peaks ① and ② of the curve of CoO, but are much different from the curve of Co_3O_4. The small peak between peaks ① and ② in the curve of Cry-Co is also induced by the silicon atoms. The results are useful to estimate the crystallinity of the samples and the analytic results are listed in Table 2.

The XAFS results indicated that each metal center has a coordination number 6 with an octahedral coordination with the surrounding atoms. The bonds of M-O-Si present in the samples Cry-Ms, and this suggests that the metal atoms are incorporated in the silica framework rather than existing as a separate oxide phase.

Preprints (www.preprints.org) | NOT PEER-REVIEWED | Posted: 18 December 2016 doi:10.20944/preprints201612.0094.v1

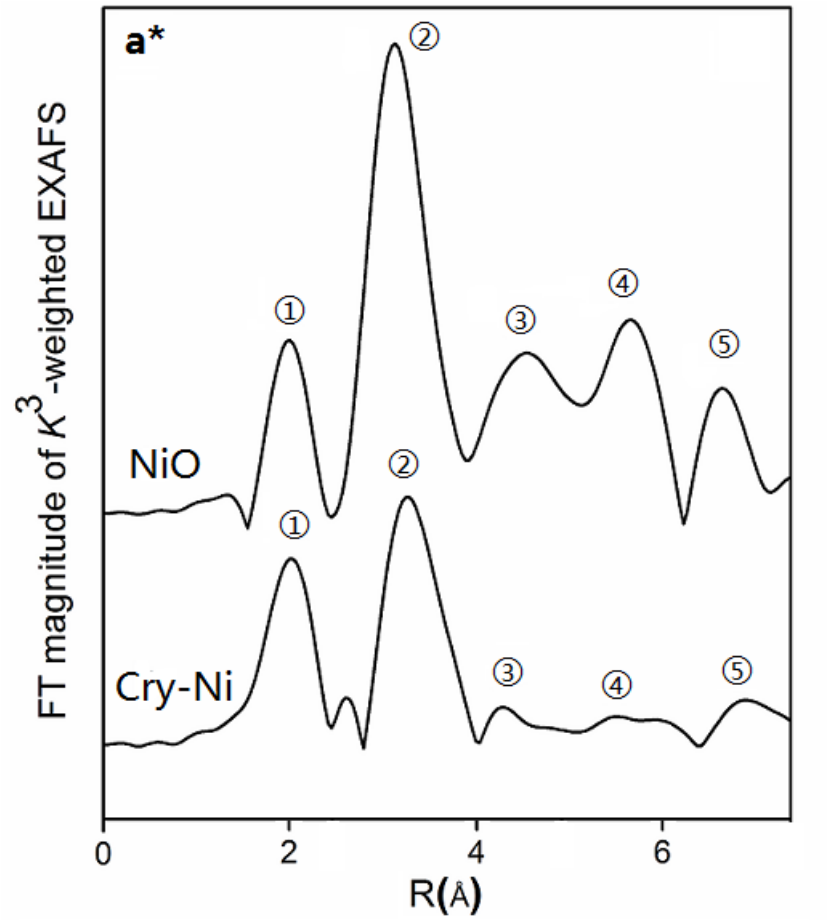

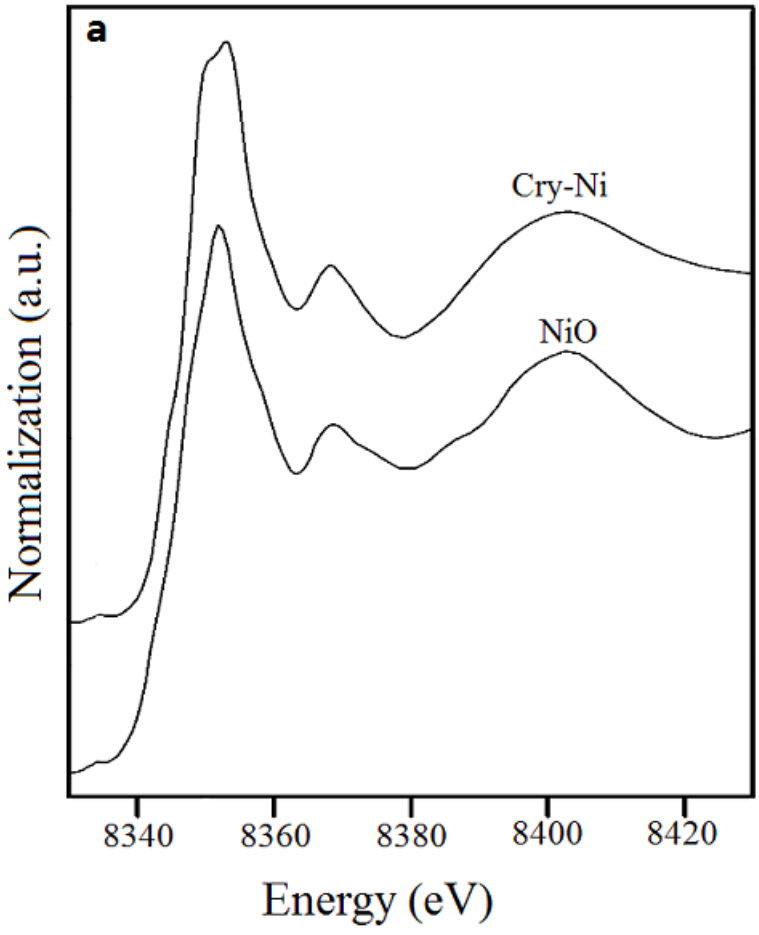

Preprints (www.preprints.org) | NOT PEER-REVIEWED | Posted: 18 December 2016 doi:10.20944/preprints201612.0094.v1

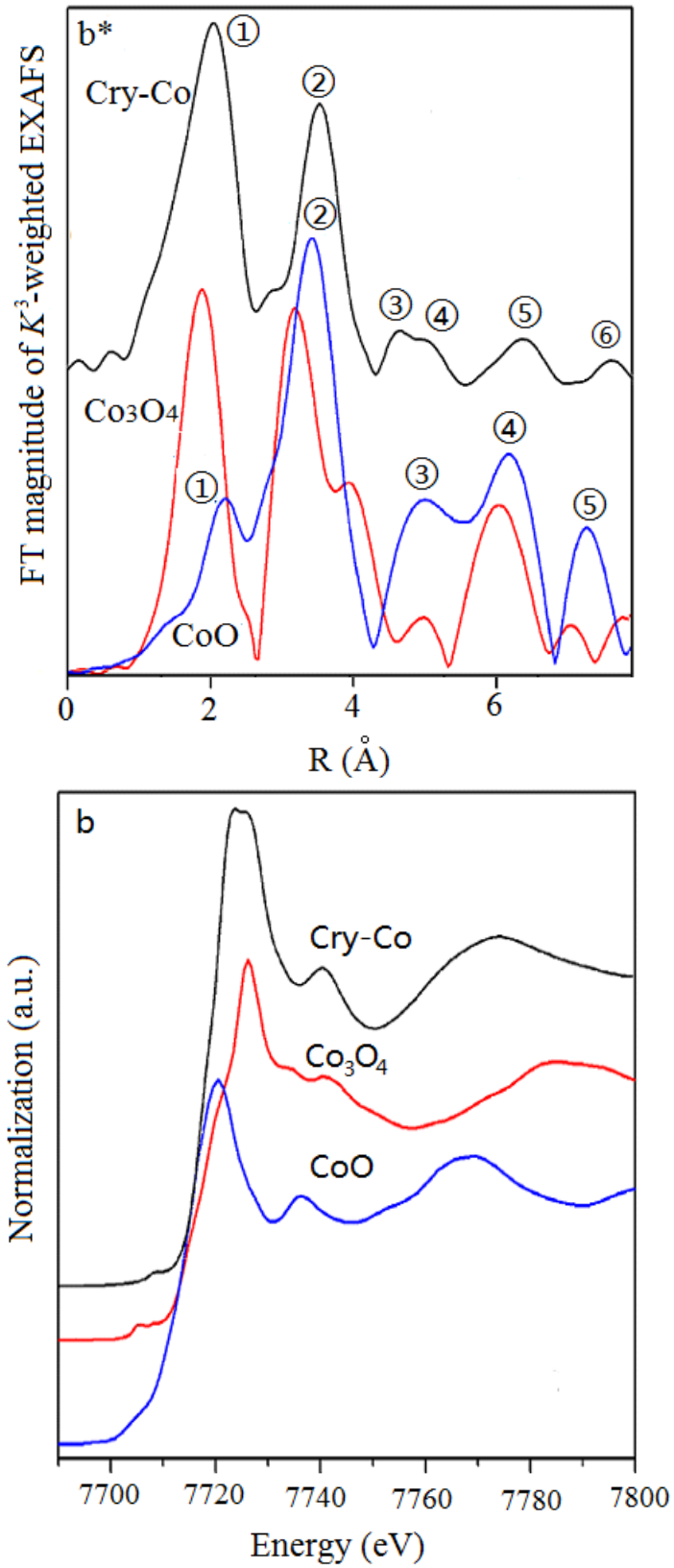

Figure 4 XANES and EXAFS of the samples: (a) Cry-Ni, (b) Cry-Co.

Table 2. EXAFS fitting results for samples.

Sample	Coordination Type	*N*	*R*(Å)	σ^2(Å^2)
Cry-N	Ni–O	6.0±0.946	2.053±0.031	0.00597±0.0008

Preprints (www.preprints.org) | NOT PEER-REVIEWED | Posted: 18 December 2016 doi:10.20944/preprints201612.0094.v1

i	Ni–Ni	12.0±0.556	3.091±0.143	0.00833±0.0008
NiO	Ni–O	6	2.084	
	Ni–Ni	12	2.948	
Cry-Co	Co-O	6.0±0.803	2.060±0.073	0.00954±0.0008
	Co-Co	12.0±0.398	3.116±0.099	0.00974±0.0008
CoO	Co-O	6	2.133	
	Co-Co	12	3.017	
Co_3O_4	Co-O	4	1.917	
	Co-Co	6	1.942	

The N_2 adsorption–desorption isotherm method was employed to investigate the pore structure of materials. The isotherms of the samples obtained at –196 °C are illustrated in Figure 5. It shows that the isotherms of the samples are type IV [23] and possess type H1 hysteresis loops. It is indicated that the samples are typical mesoporous materials, exhibiting a sharp characteristic of capillary condensation at intermediate partial pressures ($0.3 < P/P_0 < 0.5$). In the relative pressure range 0.90-0.99, all samples show another sharp with the increase of the nitrogen adsorption volume, resulting from filling the macropores formed by interparticle spaces and untrans-formed amorphous silica. The textural properties of samples were listed in Table 1. The pore diameters of the two samples have a little difference from each other, that is due to the different micelle diameter of $[(C_4H_9)_4N][M(EDTA)]$ caused by the difference radius of heteroatoms Ni^{2+} and Co^{2+}, which also influences the specific surface area, pore volume, and the pore diameter.

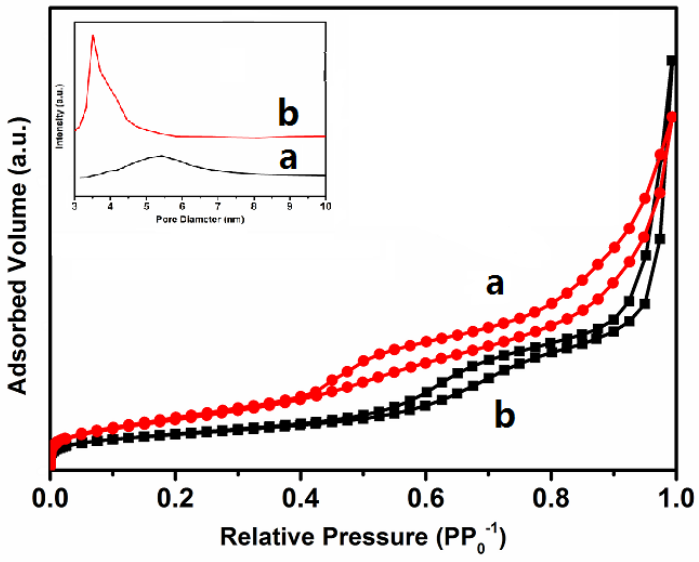

Figure 5 N_2 adsorption–desorption isotherms of the samples (inset: pore size distribution of the samples): (a) Cry-Ni, (b) Cry-Co.

 doi:10.20944/preprints201612.0094.v1

The 0.5g samples of Cry-Ni and Cry-Co were placed in 50mL 1mol/L NaOH solution, stirring at room temperature for 2 hours, then filter and dried samples. The morphological changes of the samples were observed under electron microscope, and the morphology of the samples were shown at Figure 6. The crystal structure of the samples treated by sodium hydroxide solution has been shown. The samples cover the surface of the oxide by the lye treatment has dissolved, crystal exhibits relatively complete form. Mesoporous molecular sieve material by traditional alkali treatment, hole wall collapse phenomenon will appear. In contrast, the crystal structure of metal atoms in crystalline molecular sieve improves the alkali resistance of molecular sieve.

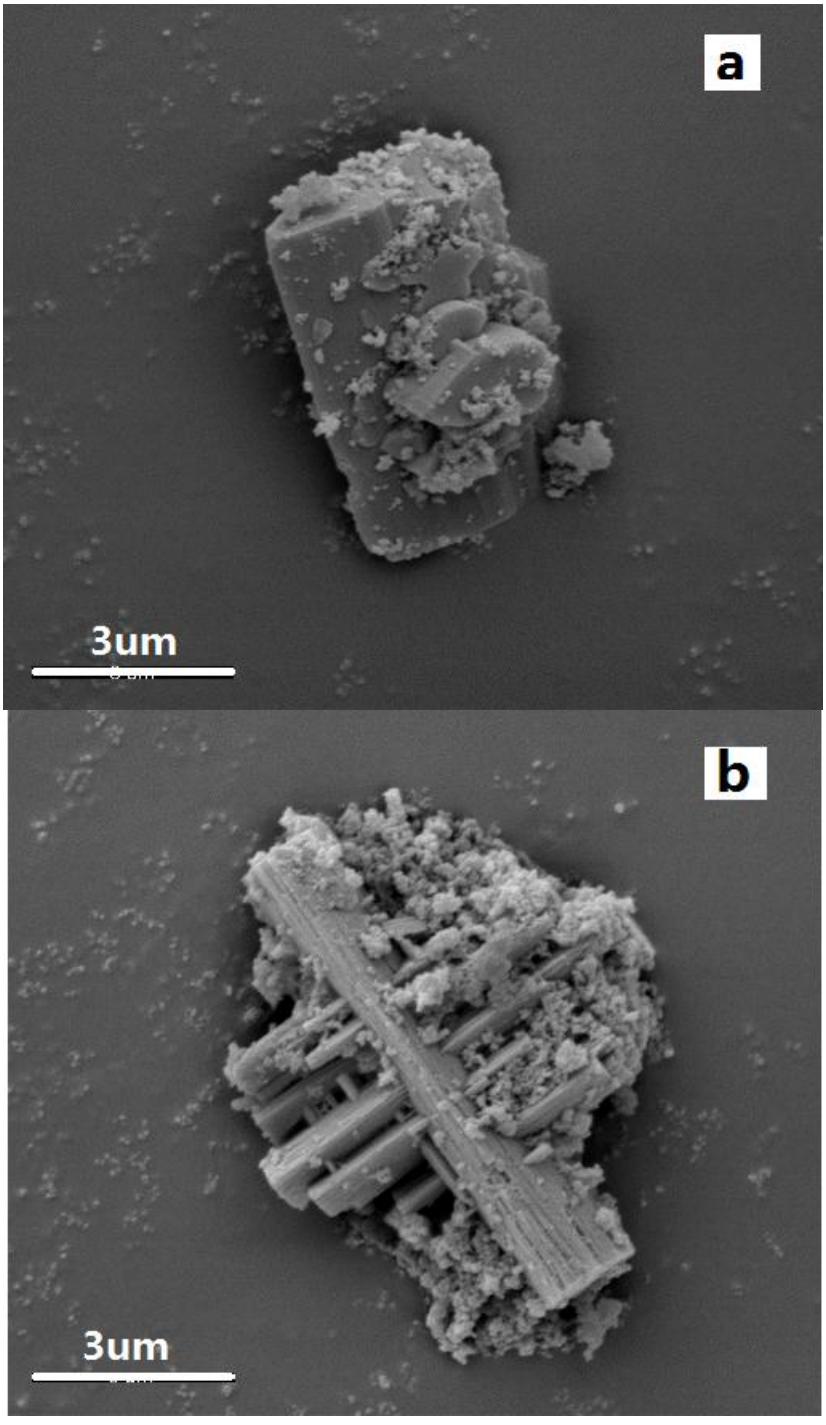

Preprints (www.preprints.org) | NOT PEER-REVIEWED | Posted: 18 December 2016 doi:10.20944/preprints201612.0094.v1

Figure 6 SEM of the samples deal with NaOH solution: (a) Cry-Ni, (b) Cry-Co.

According to the above results, a possible mechanism was proposed that is revealed as Scheme 1. There are two nitrogen atoms and four carboxyl oxygen atoms (marked as A, B, C, D, respectively) in EDTA molecule which can coordinate with the metal ion to form the complex ion $[M(EDAT)]^{2-}$ with an octahedral structure. In the chelate ion the carboxyl oxygen atoms A, B and two nitrogen atoms are at a flat surface, and the other two carboxyl oxygen atoms C and D in the vertical direction but not at a flat surface with the two nitrogen atoms. As the complex solution was added into the CTAB solution, the ionic associate $[M(EDAT)]^{2-}(CTA^{+})_2$ and the special structure micelle would be formed (Scheme 1). As the micelle suspension was mixed with the solution of SiO_4^{4-} formed by SiO_2 and plenty of sodium hydroxide, SiO_4^{4-} ions would rapidly hydrolyze and polymerize around the micelle which possessed the structure in the vertical cross directions. And the crystalline mesoporous zeolite precursors would grew up along the vertical cross directions in the following hydrothermal process. Because the structure of $[M(EDAT)]^{2-}$ complex is not same in the vertical cross directions, the micelle structure would be not same in the two directions, this is the main factor induced the sample with different structure in the different directions (Figure 2). A certain amount of the complexes formed by metal ion and EDTA was essential in the formation of the structure. The enough of $[M(EDTA)]^{2-}$ could ensure to form the single structural micelles with the vertical cross structure, which is the prerequisite of formation of the crystalline zeolite precursors.

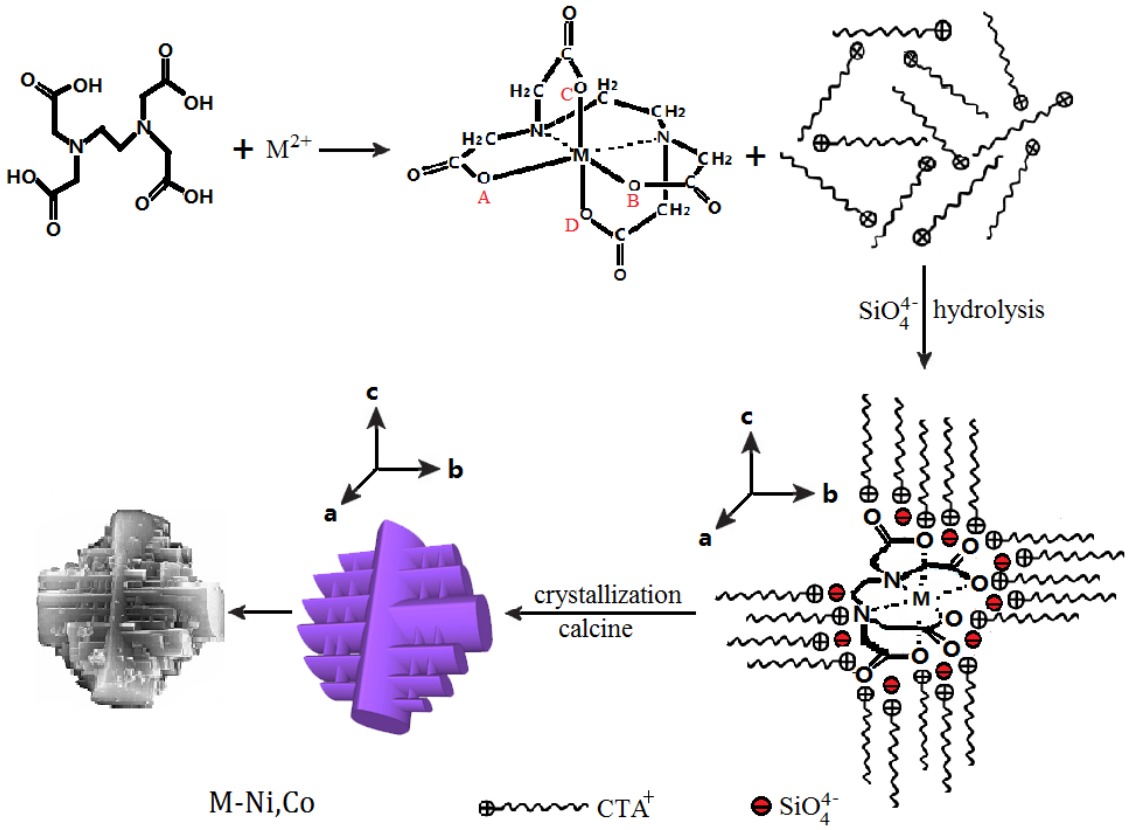

Scheme 1 The supposed formation mechanism of Cry-M.

Preprints (www.preprints.org) | NOT PEER-REVIEWED | Posted: 18 December 2016 doi:10.20944/preprints201612.0094.v1

The catalytic performance of the crystalline molecular sieves for cumene cracking has been investigated. The device diagram was shown in Figure 7. Before the reaction, the samples were activated at the temperature of 300℃and nitrogen atmosphere for one hour. Reaction conditions were as follows: temperature, 300℃; nitrogen atmosphere; mass ratio of raw material/catalyst, 100. After a certain time of reaction, the results were shown in figure 8. The first peak due to cumene peak, the second peak for small molecule hydrocarbon, the third peaks attribute to benzene homologues, it can be seen from the figure, metal atoms in the crystalline molecular sieves have a catalytic effect on the cracking of cumene. Figure a* and b* for the catalytic conversion curves, the catalytic efficiency of Cry-Ni and Cry-Co samples have not been significantly decreased after 20 times, indicating that the samples' recycling rate are higher, and the highest conversion rate of 54.5% and 44.03%. Cumene cracking reaction is a typical acid catalytic reaction. Pure silicon Si-MCM-41 molecular sieve is almost no acid, so there is no catalytic function of the reaction. Comparing to Si-MCM-41, the samples exhibited better conversion, higher selectivity for cumene cracking. The better catalytic performance is attributed to the samples possessing uniform channels, appropriate pore diameter and active sites caused by introducing Ni and Co atoms into the framework of molecular sieves.

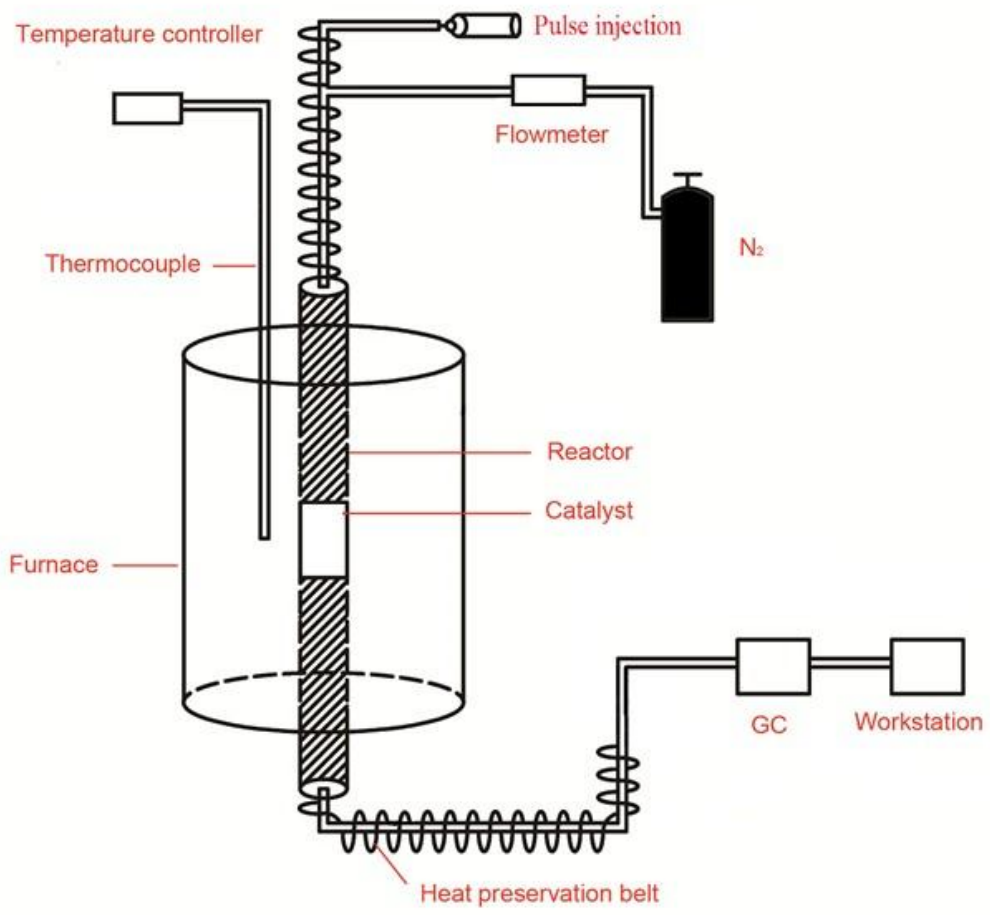

Figure 7 Diagram of apparatus for cumene cracking.

Preprints (www.preprints.org) | NOT PEER-REVIEWED | Posted: 18 December 2016 doi:10.20944/preprints201612.0094.v1

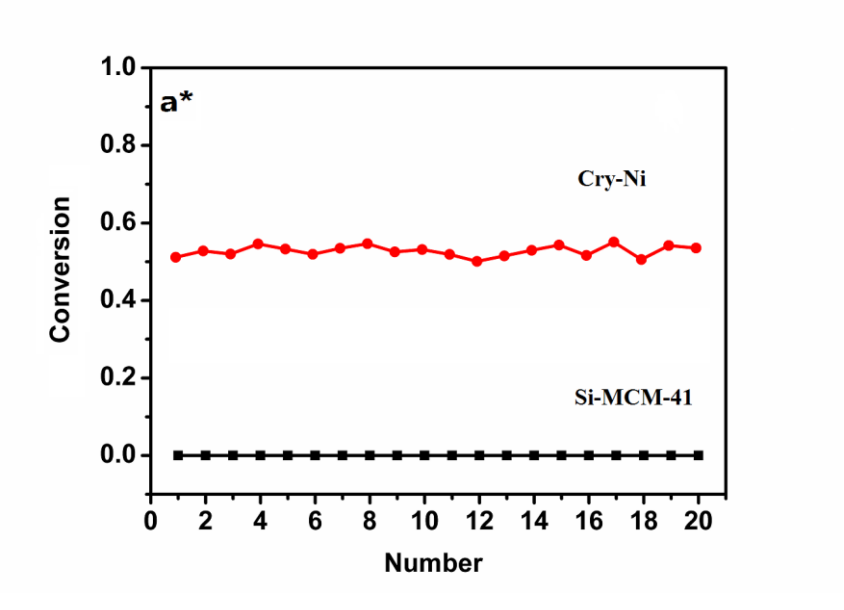

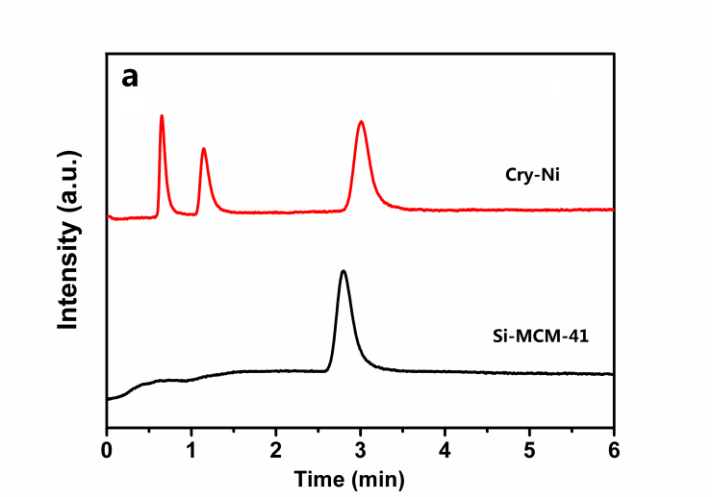

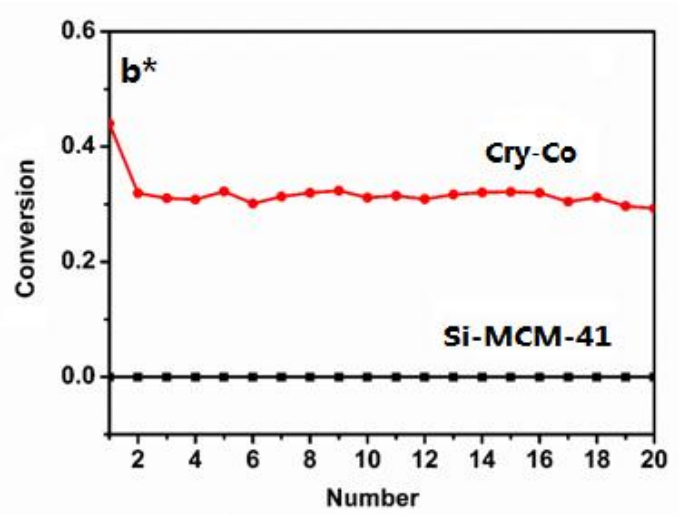

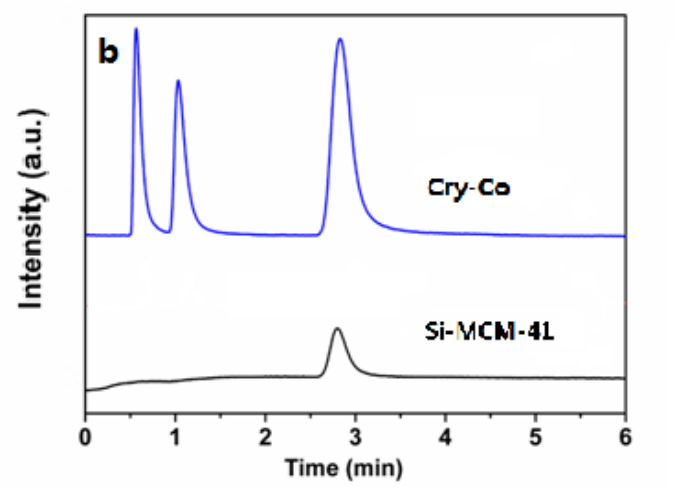

Figure 8 Chromatogram (a and a*) and conversion (b and b*) curves of the cumene cracking reaction.

4.Conclusions

The mesoporous heteroatom molecular sieve MCM-41s with the crystalline phase were synthesized via a one-step hydrothermal method. The result materials possess a structure which is in the vertical cross directions with a crystalline size of about 12 μm and high specific surface areas, and possess a highly ordered mesoporous structure and an ordered arrangement channels. The elements in the samples have a uniform distribution and highly dispersed in the materials. A certain amount of metal complexes formed by metal ion and EDTA is an essential factor for the formation of the vertical cross structure. At the same time, the crystalline mesoporous heteroatom samples improve the alkali resistance of the molecular sieves. Comparing to Si-MCM-41, the samples exhibited better conversion, higher selectivity for cumene cracking.

Reference

1. Kim, J.; Choi, M.; Ryoo, R., *J. Catal*, 269, **2010**, 219.
2. Fang, Y.; Hu, H., *J. Amer. Chem. Soc*, 128 (33), **2006**, 10636.
3. Tao, Y.; Kanoh, H.; Kaneko, K., *J. Amer. Chem. Soc*, 125, **2003**, 6044.
4. Yang, Z.; Xia, Y.; Mokaya, R., *Adv. Mater*, 16, **2004**, 727.
5. Kresge, C.; Leonowicz, M.; Roth, W.; Vartuli, J.; Beck, J., *Nature*, 359, **1992**, 710.
6. Choi, M.; Na, K.; Kim, J.; Sakamoto, Y.; Terasaki, O.; Ryoo, R., *Nature*, 461, **2009**, 246.
7. Sun, J.; Bonneau, C.; Cantín, Á.; Corma, A.; Díaz-Cabañas, M. J.; Moliner, M.; Zhang, D.; Li, M.; Zou, X., *Nature*, 458, **2009**, 1154.
8. Liu, Y.; Zhang, W.; Pinnavaia, T. J., *Angew. Chem. Int. Ed*, 11, **2001**, 1295.
9. Li, X.; Li, B.; Xu, J.; Wang, Q.; Pang, X.; Gao, X.; Zhou, Z.; Piao, J., *Appl. Clay Sci*, 50, **2010**, 81.
10. Karlsson, A.; Stöcker, M.; Schmidt, R., *Microporous Mesoporous Mater*, 27, **1999**, 181.
11. Li, B.; Li, X.; Xu J.; Pang X.; Gao X.;Zhou Z., *J. Colloid Interface Sci*, 346, **2010**, 199.
12. Li, B.; Xu, J.; Li, X.; Liu, J.; Zuo, S.; Pan, Z.; Wu, Z., *Mater. Res. Bull*, 47, **2012**, 1142.
13. Trong On, D.; Kaliaguine, S., *Angew. Chem. Int. Ed*, 113, **2001**, 3348.
14. Narkhede V.; Gies H., *Chem. Mater*, 21, **2009**, 4339.
15. Jiang, J.; Jorda, J. L.; Yu, J.; Baumes, L. A.; Mugnaioli, E.; Diaz-Cabanas, M. J.; Kolb, U.; Corma, A., *Science*, 333, **2011**, 1131.
16. Chaikittisilp,W.; Suzuki,Y.; Mukti,R. R.; Itabashi,K.; Shimojima,A.; Okubo,T., *Angew. Chem. Int. Ed.*, 125, **2013**, 3439.

17. Xuefeng Guo, Min Lai, Yan Kong, Weiping Ding, Qijie Yan, *Langmuir,* 20, **2004**, 2879.
18. Wu, N.; Zhang, W.; Li, B.; Han, C., *Microporous Mesoporous Mater,* 185, **2014**, 130.
19. Qin, J.; Li, B.; Zhang, W.; Lv, W.; Han, C.; Liu, J., *Microporous Mesoporous Mater,* 208, **2015**, 181.
20. Jamshid, I.; Donald, O.; Hossein, T., *Appl. Surf. Sci,* 185, **2001**, 72.
21. Sano, M.; Maruo, T.; Yamatera, H.; Suzuki, M.; Saito, Y., *J. Amer. Chem. Soc,* 109, **1987**, 52.
22. Guo X.; Lai M.; Kong Y.;Ding W.;Yan Q., *Langmuir,* 20, **2004**, 2879.
23. Yang, Y. H.; Lim, S.;Du, G. A.; Chen, Y.; Ciuparu, D.; Haller, G. L., *J. Phys. Chem,* 109, **2005**, 13237.